Available online at www.sciencedirect.com
ScienceDirect
Geochimica et Cosmochimica Acta 71 (2007) 5750–5762
Geochimica et Cosmochimica Acta
www.elsevier.com/locate/gca

Predicting selenite adsorption by soils using soil chemical parameters in the constant capacitance model

Sabine Goldberg *, Scott M. Lesch, Donald L. Suarez

USDA-ARS, U.S. Salinity Laboratory, 450 W. Big Springs Road, Riverside, CA 92507, USA

Received 25 October 2006; accepted in revised form 24 April 2007; available online 5 September 2007

Abstract

The constant capacitance model, a chemical surface complexation model, was applied to selenite, Se(IV), adsorption on 36 soils selected for variation in soil chemical properties. The constant capacitance model was able to fit Se(IV) adsorption by optimizing one monodentate Se(IV) surface complexation constant and the surface protonation constant. A general regression model was developed for predicting these surface complexation constants for Se(IV) from easily measured soil chemical characteristics. These chemical properties were inorganic carbon content, organic carbon content, iron oxide content, aluminum oxide content, and surface area. The prediction equations were used to obtain values for the surface complexation constants for four additional soils, thereby providing a completely independent evaluation of the ability of the constant capacitance model to describe Se(IV) adsorption. The model's ability to predict Se(IV) adsorption was quantitative on one soil and semi-quantitative on three soils. Incorporation of these prediction equations into chemical speciation–transport models will allow simulation of soil solution Se(IV) concentrations under diverse non-calcareous agricultural and environmental conditions without the requirement of soil specific adsorption data and subsequent parameter optimization.
Published by Elsevier Ltd.

1. INTRODUCTION

Selenium is both a micronutrient essential for animal nutrition and a potentially toxic trace element. The concentration range between Se deficiency and toxicity symptoms in animals is narrow. Seleniferous soils, such as occur in the Western USA, especially in South Dakota, yield enough Se to produce vegetation toxic to grazing animals (Lakin, 1961). Concentrations of Se in soils and waters can become elevated as a result of discharge from petroleum refineries, disposal of fly ash, mining activities, and mineral oxidation and dissolution (Girling, 1984). Elevated concentrations of Se in agricultural drainage waters supplying Kesterson Reservoir in the San Joaquin Valley of California caused deaths and deformities of water fowl (Ohlendorf et al., 1986). In recognition of the hazards Se poses to the welfare of animals, the U.S. Environmental Protection Agency (USEPA) has set the Se drinking water standard at a concentration of 0.633 μmol L^{-1} (50 ppb).

The dominant inorganic Se species in soil solution are selenite, Se(IV) and selenate, Se(VI) (Adriano, 1986). Selenium toxicity depends on its oxidation state with Se(IV) generally considered to be more toxic than Se(VI) (Harr, 1978; Cobo Fernandez et al., 1993). Although Se(VI) is the thermodynamically stable redox state under oxidizing conditions, the transformation rates of Se(IV) to Se(VI) are sufficiently slow that both redox states often coexist in soil solution (Masscheleyn et al., 1990).

Soil Se content is significantly positively correlated with clay, carbonate, and extractable Al and Fe oxide content (Levesque, 1974; Elsokkary, 1980). Selenium adsorption studies have been carried out on a wide range of adsorbents including oxides, clay minerals, organic matter, carbonates, and whole soils. Adsorption reactions on soil mineral surfaces can attenuate elevated soil solution Se concentrations reducing Se contamination. Selenite adsorbs strongly on soil surfaces while selenate adsorbs weakly or not at all and is readily leached to groundwater (Neal and Sposito,

* Corresponding author. Fax: +1 951 342 4962.
E-mail address: sgoldberg@ussl.ars.usda.gov (S. Goldberg).

0016-7037/$ - see front matter Published by Elsevier Ltd.
doi:10.1016/j.gca.2007.04.036

1989). Therefore, careful quantification of soil solution Se concentrations and characterization of Se(IV) adsorption on soil surfaces is needed.

Selenite adsorption on soils and soil minerals has been described using various modeling approaches. Such models include the empirical distribution coefficient, K_d (Fujikawa and Fukui, 1997; Wang and Liu, 2005), Freundlich (Del Debbio, 1991), and Langmuir (Elsokkary, 1980; Singh et al., 1981; Saeki and Matsumoto, 1994) adsorption isotherm equations, and surface complexation models: constant capacitance model (Goldberg and Glaubig, 1988; Sposito et al., 1988; Anderson and Benjamin, 1990a,b; Duc et al., 2003, 2006), diffuse layer model (Dzombak and Morel, 1990; Balistrieri et al., 2003), triple layer model (Hayes et al., 1988; Balistrieri and Chao, 1990; Zhang and Sparks, 1990; Ghosh et al., 1994; Martinez et al., 2006), and charge distribution multisite complexation, CD-MUSIC, model (Hiemstra and van Riemsdijk, 1999). Parameters obtained from adsorption isotherm equations are empirical and only valid for the conditions under which the experiment was conducted. Chemical surface complexation models define surface species, chemical reactions, mass balances, and charge balances and contain molecular features that can be given thermodynamic significance (Sposito, 1983).

Selenite has been observed spectroscopically to adsorb specifically on the iron oxides, goethite (Hayes et al., 1987; Manceau and Charlet, 1994), hematite (Catalano et al., 2006), and amorphous iron oxide (Manceau and Charlet, 1994), on the aluminum oxides, gibbsite, corundum (Papelis et al., 1995; Peak, 2006), and amorphous aluminum oxide (Peak, 2006), on the manganese oxides, vernadite and birnessite (Foster et al., 2003), and on the clay mineral montmorillonite (Peak et al., 2006) forming strong inner-sphere surface complexes containing no water between the adsorbing Se(IV) ion and the surface functional group. Selenite was found to adsorb on hematite (Catalano et al., 2006) amorphous aluminum oxide (Peak, 2006), and montmorillonite (Peak et al., 2006) as bidentate surface complexes. A mixture of monodentate and bidentate Se(IV) surface complexes was observed on manganese oxide (Foster et al., 2003).

All surface complexation modeling approaches indicated above postulated monodentate inner-sphere surface complexes for Se(IV) adsorption, with the exception of the study of Balistrieri and Chao (1990) which considered a bidentate surface complex on goethite and the study of Hiemstra and van Riemsdijk (1999) which considered a combination of mono- and bidentate surface complexes on goethite. Duc et al. (2006) found that the fits obtained with the constant capacitance model were of comparable quality when using either a monodentate or a bidentate surface configuration. Chemical modeling of Se(IV) adsorption has been carried out on heterogeneous natural materials for the clay minerals, kaolinite and montmorillonite (Goldberg and Glaubig, 1988) and soils using monodentate surface complexes in the constant capacitance model (Goldberg and Glaubig, 1988; Sposito et al., 1988).

The predictive capability of the constant capacitance model to describe trace element adsorption has been tested (Goldberg et al., 2000, 2002, 2004, 2005). A general regression model was used to predict model surface complexation constants from easily measured soil chemical properties such as: surface area, cation exchange capacity, organic carbon content, inorganic carbon content, aluminum oxide content, and iron oxide content. This approach provided a completely independent model evaluation and was able to predict borate (Goldberg et al., 2000, 2004), molybdate (Goldberg et al., 2002), and arsenate (Goldberg et al., 2005) adsorption on numerous diverse soils having a wide range of chemical characteristics.

The objectives of the present study are: (i) to apply the constant capacitance model to Se(IV) adsorption on a set of 45 soil samples using both monodentate and bidentate surface configurations for adsorbed Se(IV); (ii) to relate Se(IV) adsorption characteristics and model surface complexation constants to easily measured chemical parameters affecting Se(IV) adsorption such as surface area (SA), cation exchange capacity (CEC), organic carbon content (OC), inorganic carbon content (IOC), aluminum oxide content (Al), and iron oxide content (Fe); (iii) to relate quantitatively variations in these soil properties to variations in values of the surface complexation constants obtained by the constant capacitance model; and (iv) to evaluate the ability of the constant capacitance model to predict Se(IV) adsorption on additional soils using the surface complexation constants calculated from soil chemical properties.

2. EXPERIMENTAL SECTION

Selenite adsorption was investigated using 45 surface and subsurface soil samples from 36 soil series belonging to six different soil orders. The soils were chosen to cover a wide range of chemical characteristics. Soil classifications and chemical characteristics are provided in Table 1. The Southeastern soil subgroup (the first 20 soil series listed: Altamont to Yolo) constitutes a group of soils primarily from California that had been used in prior studies of borate (Goldberg et al., 2000), molybdate (Goldberg et al., 2002), and arsenate (Goldberg et al., 2005) adsorption. This set of soils consists mainly of alfisols and entisols with some vertisols, mollisols, an inceptisol, and an aridisol. The Midwestern subgroup (the following 16 soil series listed: Bernow to Teller) constitutes a group of soils from Iowa and Oklahoma that had been used in prior studies of borate (Goldberg et al., 2004), and arsenate adsorption (Goldberg et al., 2005). This set of soils consists mainly of mollisols with some alfisols and vertisols. The Southwestern soils exhibit a higher range in pH value, consistent with the lower rainfall amounts experienced in this part of the country over those experienced by the Midwestern soils.

Soil pH values were measured in deionized water at a soil to water ratio of 1:5 as described by Thomas (1996). Cation exchange capacities were measured by the Na saturation and Mg extraction method for arid-zone soils (Rhoades, 1982). Surface areas were determined by adsorption of ethylene glycol monoethyl ether (EGME) as described by Cihacek and Bremner (1979). Free Fe and Al were extracted using a Na citrate/citric acid buffer and Na hydrosulphite (Coffin, 1963) and measured using inductively

Table 1
Classifications and chemical characteristics of soils

Soil series	Depth (cm)	pH	CEC ($mmol_c\ kg^{-1}$)	SA ($km^2\ kg^{-1}$)	IOC ($g\ kg^{-1}$)	OC ($g\ kg^{-1}$)	Fe ($g\ kg^{-1}$)	Al ($g\ kg^{-1}$)
Southwestern soils								
Altamont (fine, smectitic, thermic Aridic Haploxerert)	0–23	6.17	179	0.109	0.12	30.8	9.2	0.88
Arlington (coarse-loamy, mixed thermic Haplic Durixeralf)	0–25	8.25	107	0.0611	0.30	4.7	8.2	0.48
Avon (fine, smectitic, mesic, calcic Pachic Argixeroll)	0–15	6.85	183	0.0601	0.083	30.8	4.3	0.78
Bonsall (fine, smectitic, thermic Natric Palexeralf)	0–25	5.92	54	0.0157	0.13	4.9	9.3	0.45
Chino (fine-loamy, mixed, thermic Aquic Haploxeroll)	0–15	10.1	304	0.159	6.4	6.2	4.7	1.64
Diablo (fine, smectitic, thermic Aridic Haploxerert)	0–15	8.01	301	0.19	0.26	19.8	7.1	1.02
	0–15	7.47	234	0.13	2.2	28.3	5.8	0.84
Fallbrook (fine-loamy, mixed, thermic Typic Haploxeralf)	25–51	6.27	78	0.0285	0.24	3.1	4.9	0.21
Fiander (fine-silty, mixed, mesic Typic Natraquoll)	0–15	9.60	248	0.0925	6.9	4.0	9.2	1.06
Haines (coarse-silty, mixed, calcareous, mesic Typic Haplaquept)	20	9.07	80	0.0595	15.8	14.9	1.7	0.18
Hanford (coarse-loamy, mixed, non-acid, thermic Typic Xerorthent)	0–10	8.24	111	0.0289	10.1	28.7	6.6	0.35
Holtville (clayey over loamy, smectitic, mixed, calcareous, hyperthermic Typic Torrifluvent)	61–76	8.82	58	0.043	16.4	2.1	4.9	0.27
Imperial (fine, smectitic, calcareous, hyperthermic Vertic Torrifluvent)	15–46	8.53	198	0.106	17.9	4.5	7.0	0.53
Nohili (very-fine, smectitic, calcareous, isohyperthermic Cumulic Endoaquoll)	0–23	8.01	467	0.286	2.7	21.3	49.0	3.7
Pachappa (coarse-loamy, mixed, thermic Mollic Haploxeralf)	0–25	6.84	39	0.0151	0.026	3.8	7.6	0.67
	25–51	7.03	52	0.041	0.014	1.1	7.2	0.35
	0–20	9.40	122	0.0858	0.87	3.5	5.6	0.86
Porterville (fine, smectitic, thermic Aridic Haploxerert)	0–7.6	6.76	203	0.137	0.039	9.4	10.7	0.90
Reagan (fine-silty, mixed, thermic Ustic Haplocalcid)	Surface	8.34	98	0.0588	18.3	10.1	4.6	0.45
Sebree (fine-silty, mixed, mesic Xerollic Nadurargid)	0–13	5.69	27	0.0212	0.0063	2.2	6.0	0.46
Wasco (coarse-loamy, mixed, non-acid, thermic Typic Torriorthent)	0–5.1	4.51	71	0.0309	0.009	4.7	2.4	0.42
Wyo (fine-loamy, mixed, thermic Mollic Haploxeralf)		6.37	155	0.0539	0.014	19.9	9.5	0.89
Yolo (fine-silty, mixed, non-acid, thermic Typic Xerorthent)	0–15	8.43	177	0.0730	0.23	11.5	15.6	1.13
Midwestern soils								
Bernow (fine-loamy, siliceous, thermic Glossic Paleudalf)	B	3.87	77.6	0.0464	0.0028	3.8	8.1	1.1
Canisteo (fine-loamy, mixed, superactive, calcareous, mesic Typic Endoaquoll)	A	7.99	195	0.152	14.8	34.3	1.7	0.44
Dennis (fine, mixed, thermic Aquic Argiudoll)	A	4.81	85.5	0.0403	0.0014	18.6	12.9	1.7
	B	5.29	63.1	0.0724	0.0010	5.2	30.0	4.1
Dougherty (loamy, mixed, active, thermic Arenic Haplustalf)	A	4.76	3.67	0.241	0.0010	7.0	1.7	0.28
Hanlon (coarse-loamy, mixed, superactive, mesic Cumulic Hapludoll)	A	7.56	142	0.0587	2.6	15.1	3.7	0.45
Kirkland (fine, mixed, superactive, thermic Udertic Paleustoll)	A	5.02	154	0.0421	0.014	12.3	5.6	0.80
Luton (fine, smectitic, mesic Typic Endoaquert)	A	7.05	317	0.169	0.099	21.1	9.1	0.99
Mansic (fine-loamy, mixed, superactive, thermic Aridic Calciustoll)	A	8.38	142	0.0422	16.7	10.1	2.7	0.40
	B	8.78	88.1	0.0355	63.4	9.0	1.1	0.23
Norge (fine-silty, mixed, active, thermic Udic Paleustoll)	A	3.65	62.1	0.0219	0.0010	11.6	6.1	0.75
Osage (fine, smectitic, thermic Typic Epiaquert)	A	7.04	377	0.134	0.59	29.2	15.9	1.4
	B	6.43	384	0.143	0.0100	18.9	16.5	1.3

Table 1 (*continued*)

Soil series	Depth (cm)	pH	CEC ($mmol_c\ kg^{-1}$)	SA ($km^2\ kg^{-1}$)	IOC ($g\ kg^{-1}$)	OC ($g\ kg^{-1}$)	Fe ($g\ kg^{-1}$)	Al ($g\ kg^{-1}$)
Pond Creek (fine-silty, mixed, superactive, thermic Pachic Argiustoll)	A	4.82	141	0.0354	0.0023	16.6	5.2	0.70
	B	6.15	106	0.0596	0.016	5.0	5.1	0.81
Pratt (sandy, mixed, mesic Lamellic Haplustalf)	A	5.94	23.9	0.0123	0.0026	4.2	1.2	0.18
	B	5.74	23.3	0.117	0.0007	2.1	0.92	0.13
Richfield (fine, smectitic, mesic Aridic Argiustoll)	B	7.38	275	0.082	0.040	8.0	5.4	0.76
Summit (fine, smectitic, thermic Oxyaquic Vertic Argiudoll)	A	7.46	374	0.218	0.25	26.7	16.2	2.3
	B	6.84	384	0.169	0.0079	10.3	17.8	2.5
Taloka (fine, mixed, thermic Mollic Albaqualf)	A	4.90	47.4	0.087	0.0021	9.3	3.6	0.62
Teller (fine-loamy, mixed, active, thermic Udic Argiustoll)	A	3.67	43.1	0.227	0.0008	6.8	3.2	0.53

CEC, cation exchange capacity; SA, surface area; IOC, inorganic carbon; OC, organic carbon.

coupled plasma (ICP) emission spectrometry. Carbon contents were determined using a carbon coulometer[1] (UIC, Inc., Joliet, IL). Organic carbon was obtained by the difference between total carbon determined by furnace combustion at 950 °C and inorganic carbon determined using an acidification module and heating. The soil samples represented a broad range of chemical characteristics: pH: 3.7–10.1, CEC: 3.7–467 $mmol_c\ kg^{-1}$, SA: 0.0123–0.286 $km^2\ kg^{-1}$, IOC: 0.0007–63 $g\ kg^{-1}$, OC: 1.1–34 $g\ kg^{-1}$, Fe: 0.9–49 $g\ kg^{-1}$, Al: 0.13–4.1 $g\ kg^{-1}$ (see Table 1).

Selenite adsorption experiments were carried out in batch systems to determine adsorption envelopes (amount of Se(IV) adsorbed as a function of solution pH at fixed total Se(IV) mass). One gram of soil was added to 50-mL polypropylene centrifuge tubes and equilibrated with 25 mL of a 0.1 M NaCl solution by shaking on a reciprocating shaker for 2 h. This reaction time was used in a prior study of Se(IV) adsorption by soil (Goldberg and Glaubig, 1988). The equilibrating solution contained 20 $\mu mol\ L^{-1}$ Se(IV) and had been adjusted to the desired pH range of 2–10 using 1.0 M HCl or 1.0 M NaOH. After reaction, the samples were centrifuged and the decantates analyzed for pH, passed through 0.45 μm membrane filters, and analyzed for Se concentration using ICP spectrometry. Initial analyses using the direct speciation method of Goldberg et al. (2006) verified that no oxidation of Se(IV) to Se(VI) had occurred.

Carbonates were removed from subsamples of the Holtville, Imperial, and Reagan soils using a modification of the procedure described by Kunze and Dixon (1986). The soils were washed three times with 0.5 M Na acetate which had been adjusted to pH 5 with glacial acetic acid, washed twice with deionized water, air dried, and passed through a 2-mm sieve. The chemical properties of the treated subsamples were characterized and their Se(IV) adsorption behavior determined under identical conditions as described above.

A detailed discussion of the theory and assumptions of the constant capacitance surface complexation model is available (Goldberg, 1992). In the present application of the model to Se(IV) adsorption, the following surface complexation constants were considered:

$$SOH_{(s)} + H^+_{(aq)} \rightleftharpoons SOH^+_{2(s)} \quad (1)$$

$$SOH_{(s)} \rightleftharpoons SO^-_{(s)} + H^+_{(aq)} \quad (2)$$

$$SOH_{(s)} + H_2SeO_{3(aq)} \rightleftharpoons SHSeO_{3(s)} + H_2O \quad (3)$$

$$SOH_{(s)} + H_2SeO_{3(aq)} \rightleftharpoons SSeO^-_{3(s)} + H^+_{(aq)} + H_2O \quad (4)$$

$$2SOH_{(s)} + H_2SeO_{3(aq)} \rightleftharpoons S_2SeO_{3(s)} + 2H_2O \quad (5)$$

where $SOH_{(s)}$ represents reactive surface hydroxyl groups on oxide minerals and aluminol groups on clay minerals in the soils. By convention, surface complexation reactions in the constant capacitance model are written starting with the completely undissociated acids; however, the model application contains the aqueous speciation reactions for Se(IV). Both monodentate and bidentate Se(IV) surface species were considered, consistent with spectroscopic observations.

Intrinsic equilibrium constants for the surface complexation reactions are:

$$K_+(\text{int}) = \frac{[SOH_2^+]}{[SOH][H^+]} \exp(F\psi/RT) \quad (6)$$

$$K_-(\text{int}) = \frac{[SO^-][H^+]}{[SOH]} \exp(-F\psi/RT) \quad (7)$$

$$K^1_{Se}(\text{int}) = \frac{[SHSeO_3]}{[SOH][H_2SeO_3]} \quad (8)$$

$$K^2_{Se}(\text{int}) = \frac{[SSeO_3^-][H^+]}{[SOH][H_2SeO_3]} \exp(-F\psi/RT) \quad (9)$$

$$K^3_{Se}(\text{int}) = \frac{[S_2SeO_3]}{[SOH]^2[H_2SeO_3]} \quad (10)$$

where square brackets indicate concentrations ($mol\ L^{-1}$), F is the Faraday constant ($C\ mol_c^{-1}$), ψ is the surface potential

[1] Trade names and company names are included for the benefit of the reader and do not imply any endorsement or preferential treatment of the product listed by the U.S. Department of Agriculture.

(V), R is the molar gas constant (J mol^{-1} K^{-1}), and T is the absolute temperature (K). The exponential terms can be considered as solid-phase activity coefficients that correct for charge on the surface complexes. The assumption is made that the number of bidentate sites, $\equiv S_2$, is equal to one half that of the monodentate sites, $\equiv S$. However, the number of bidentate sites available for Se(IV) adsorption is actually less than that because the two monodentate sites used to form the bidentate Se(IV) surface complex must be adjacent to each other (Benjamin, 2002). In the present application, surface complexation constants for monodentate and bidentate Se(IV) surface species will be determined in separate optimizations.

Mass balance of the surface functional groups for monodentate adsorption only is:

$$[\mathrm{SOH}]_T = [\mathrm{SOH}] + [\mathrm{SOH}_2^+] + [\mathrm{SO}^-] + [\mathrm{SHSeO}_3] + [\mathrm{SSeO}_3^-] \quad (11)$$

and mass balance for bidentate adsorption only is:

$$[\mathrm{SOH}]_T = [\mathrm{SOH}] + [\mathrm{SOH}_2^+] + [\mathrm{SO}^-] + 2[\mathrm{S_2SeO_3}] \quad (12)$$

Charge balance for monodentate adsorption only is:

$$\sigma = [\mathrm{SOH}_2^+] - [\mathrm{SO}^-] - [\mathrm{SSeO}_3^-] \quad (13)$$

and charge balance for bidentate adsorption only is:

$$\sigma = [\mathrm{SOH}_2^+] - [\mathrm{SO}^-] \quad (14)$$

where σ has units of (mol$_c$ L^{-1}).

The computer program FITEQL 3.2 (Herbelin and Westall, 1996) was used to fit surface complexation constants to the experimental adsorption data. The program uses a nonlinear least squares optimization routine to fit equilibrium constants to experimental data and contains the constant capacitance model for surface complexation. FITEQL can also be used to calculate and predict chemical speciation using equilibrium constant values determined from previous experiments. The assumption that Se(IV) adsorption takes place on only one set of reactive surface functional groups is clearly a gross simplification since soils are complex multisite mixtures containing many diverse surface sites. Selenite surface complexation constants determined for soils are average composite values that include competing ion effects and soil mineralogical characteristics.

Initial input parameter values for the model were: surface area, capacitance: $C = 1.06$ F m^{-2} (considered optimum for Al oxide by Westall and Hohl, 1980), protonation constant: $\log K_+(\mathrm{int}) = 7.35$, deprotonation constant: $\log K_-(\mathrm{int}) = -8.95$ (averages of a literature compilation for Al and Fe oxides by Goldberg and Sposito, 1984), and total number of reactive surface hydroxyl groups: $N_S = 2.31$ sites nm^{-2} (recommended for natural materials by Davis and Kent, 1990). Previous sensitivity analyses showed that surface complexation modeling was highly dependent on surface site density (Goldberg, 1991), but more than tripling the capacitance produced only minor changes in the values of the surface complexation constants (Goldberg and Sposito, 1984). It is necessary to maintain constant values of capacitance and surface site density so that the model results can be used to predict Se(IV) adsorption by additional soils. The goodness-of-fit parameter was the overall variance V in Y:

$$V_Y = \frac{\mathrm{SOS}}{\mathrm{DF}} \quad (15)$$

where SOS is the weighted sum of squares of the residuals and DF is the degrees of freedom.

The initial, fully specified functions for each surface complexation constant were defined to be:

$$\log K_j(\mathrm{int}) = \beta_{0j} + \beta_{1j}(\ln \mathrm{CEC}_i) + \beta_{2j}(\ln \mathrm{SA}_i) + \beta_{3j}(\ln \mathrm{IOC}_i) + \beta_{4j}(\ln \mathrm{OC}_i) + \beta_{5j}(\ln \mathrm{Fe}_i) + \beta_{6j}(\ln \mathrm{Al}_i) + \varepsilon_i \quad (16)$$

where $\log K(\mathrm{int})$ represents the specific surface complexation constant, $j = 1$ (Southwestern) or 2 (Midwestern) soil groups, and ε (the residual error term) is assumed to follow the usual regression modeling assumptions of Normal errors. Note that Eq. (16) represents an analysis of covariance (ANOCOVA) model which can be recast as a multivariate analysis of covariance (MANOCOVA) model, if one desires to perform tests across both sets of estimated (surface complexation constant) regression model parameters simultaneously. For this analysis, the goal of the model building process was to determine the best set of reduced regression model parameters for predicting these surface complexation constants.

The model building process proceeded in three stages. First, the MANOCOVA version of Eq. (16) was estimated so that a joint parameter test (Wilks' lambda) could be performed (Johnson and Wichern, 1988). This test was used to verify that at least some of the model parameter estimates were statistically different across the two soil groups. Eq. (16) was then analyzed separately for each surface complexation constant using a backwards elimination (BWE) procedure, where the critical cut-off p-value used for parameter removal was set to $\alpha = 0.15$ (Myers, 1986). Based on the results from this BWE procedure, a reduced prediction equation was specified for each surface complexation constant. Specifically, if the BWE procedure removed the same regression variable from both soil groups, then this variable was left out of the reduced equation (otherwise the variable was retained for each group).

In the third and final stage of the model development process, the jack-knifed prediction error (PRESS statistic) was first calculated for the reduced equation and then the remaining group-specific model parameters were sequentially deleted and/or pooled across groups in an effort to improve (i.e., reduce) the PRESS statistic (Myers, 1986). In this process, each remaining parameter could be (i) deleted jointly across both soil groups, (ii) pooled across soil groups (i.e., made into a common parameter), or (iii) set to 0 for just one soil group (i.e., deleted for one soil group only). However, when any parameters were deleted, they were always deleted jointly (across both soil groups) unless the corresponding p-values clearly indicated a dichotomous effect; i.e., one p-value >0.5 and another <0.05. This process continued until the PRESS statistic was minimized; i.e., the jack-knifed prediction variance was made as small as possible. All multivariate analysis of variance (ANOVA) tests,

regression model development, and prediction error analyses were carried out using SAS software (SAS, 1999).

3. RESULTS AND DISCUSSION

Selenite adsorption as a function of solution pH was determined for 45 different soil samples (examples are presented in Figs. 1 and 2). Selenite adsorption generally decreased with increasing solution pH. The decrease in adsorption was observed at a much higher pH value for the Midwestern soils (Fig. 2) than the Southwestern soils (Fig. 1).

The constant capacitance model was fit to the Se(IV) adsorption envelopes of all the soil samples. Surface complexation constants for both monodentate and bidentate surface configurations of adsorbed Se(IV) were optimized in separate calculations. Model fits were superior in quality (as measured by the goodness-of-fit criterion, V_Y) when monodentate Se(IV) surface species were used ($\overline{V_Y} = 9.5$ for monodentate, $\overline{V_Y} = 10.4$ for bidentate). Simultaneous optimization of the two monodentate surface complexation constants, $\log K^1_{Se}(\text{int})$ and $\log K^2_{Se}(\text{int})$ was only possible for five of the soils. For all other soils, only the constant for the negatively charged Se(IV) surface species, $\log K^2_{Se}(\text{int})$, was optimized since $\log K^1_{Se}(\text{int})$ did not converge. To improve the model fit, values of the protonation constant, $\log K_+(\text{int})$, and the deprotonation constant, $\log K_-(\text{int})$, were simultaneously optimized with the Se(IV) constant, $\log K^2_{Se}(\text{int})$. Results of the initial optimizations indicated that the deprotonated species was only required in trace amounts ($\log K_-(\text{int}) < -38.95$). It was therefore omitted from the final optimizations. Table 2 provides final values for the optimized surface complexation constants. Optimized constants are not listed for the soils having >1.4% inorganic carbon content since the constant capacitance model could not converge $\log K^2_{Se}(\text{int})$ and $\log K_+(\text{int})$ simultaneously under these circumstances. Simultaneous optimization of $\log K_{Se}(\text{int})$, $\log K_+(\text{int})$, and $\log K_-(\text{int})$ was possible for only two soils using a bidentate Se(IV) surface configuration. Therefore, the bidentate approach was not pursued further.

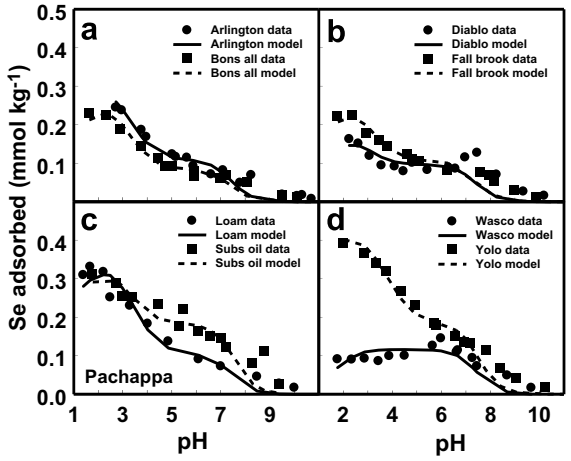

Fig. 1. Fit of the constant capacitance model to Se(IV) adsorption by Southwestern soils. Experimental data are represented by circles and by squares. Model fits are represented by solid and dashed lines.

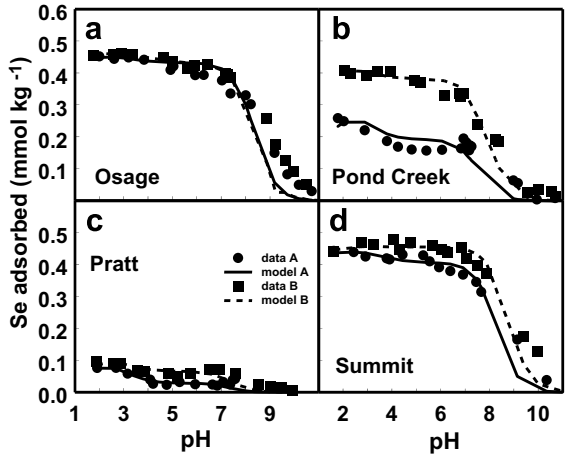

Fig. 2. Fit of the constant capacitance model to Se(IV) adsorption by Midwestern soils: (a) Osage soil; (b) Pond Creek soil; (c) Pratt soil; and (d) Summit soil. Experimental data are represented by circles for the A horizons and by squares for the B horizons. Model fits are represented by solid lines for the A horizons and dashed lines for the B horizons.

Figs. 1 and 2 indicate the ability of the constant capacitance model to describe Se(IV) adsorption on 16 soils by simultaneously optimizing $\log K^2_{Se}(\text{int})$ and $\log K_+(\text{int})$. The model generally provided a good description of the adsorption data up to a solution pH of 7–8. At higher pH values, the adsorption data were under-predicted. We chose a representative subset of soils for presentation in these figures. For the Midwestern soils (Fig. 2), we chose to present the soils for which we were able to determine Se(IV) adsorption envelopes on both surface and subsurface horizons. The range in quality of model fits is well representative of both sets of soils studied. For each Midwestern soil, the model fit was comparable in quality for both horizons. The quality of fit for the Midwestern soils (Fig. 2) was better than that for the Southwestern soils (Fig. 1).

A general regression modeling approach was used to relate the Se(IV) surface complexation constants to the following set of soil chemical properties: CEC, SA, IOC, OC, Fe, and Al. The 35 soils used to obtain the regression model results discussed below had the following ranges of soil properties: CEC: 3.7–384 $\text{mmol}_c\ \text{kg}^{-1}$, SA: 0.0123–0.241 $\text{km}^2\ \text{kg}^{-1}$, IOC: 0.0007–10.1 g kg^{-1}, OC: 1.1–30.8 g kg^{-1}, Fe: 1.1–17.8 g kg^{-1}, and Al: 0.13–2.5 g kg^{-1}.

Upon visual inspection, the average levels of the numerically optimized surface complexation constants appeared to be different across the two soil groups (Midwestern and Southwestern, respectively). This difference was confirmed using a multivariate Hotelling's T^2 test ($F = 7.01$, $p = 0.003$). A second multivariate parameter test (MANOCOVA model parameter test: $F = 5.35$, $p < 0.001$) confirmed that the estimated regression model parameters also appeared to change across soil groups (Johnson and

Table 2
Constant capacitance model surface complexation constants

Soil series	Depth (cm)	Fitted $\log K^2_{Se}$	Fitted $\log K_+$	Predicted $\log K^2_{Se}$	Predicted $\log K_+$	Jack-knife predicted $\log K^2_{Se}$	Jack-knife predicted $\log K_+$	Average absolute error
Southwestern soils								
Altamont	0–20	−1.42	2.72	−1.23	2.79	−1.18	2.80	0.16
Arlington	0–25	−1.04	2.82	−0.88	2.81	−0.87	2.80	0.09
Avon	0–15	−1.24	2.27	−1.21	2.16	−1.20	2.14	0.09
Bonsall	0–25	−0.90	2.80	−0.62	2.81	−0.57	2.81	0.17
Chino	0–15	−1.57	2.96	−1.42	2.72	−1.40	2.64	0.24
Diablo	0–15	−1.57	2.11	−1.47	2.68	−1.46	2.71	0.35
	0–15	−1.75	2.85	−1.41	2.77	−1.34	2.75	0.25
Fallbrook	25–51	−0.73	2.53	−0.70	2.38	−0.69	2.37	0.10
Fiander	0–15	−1.01	3.20	−0.99	3.25	−0.99	3.27	0.04
Haines	20	NC[a]	NC	−1.40	2.04			
Hanford	0–10	−0.53	2.68	−0.81	3.04	−0.89	3.15	0.41
Holtville	61–76	NC	NC	−0.82	2.87			
Imperial	15–46	NC	NC	−1.13	3.15			
Nohili	0–23	NC	NC	−1.10	4.44			
Pachappa	0–25		2.17	−0.69	2.47	−0.69	2.50	
	25–51	−0.53	2.50	−0.65	2.35	−0.70	2.33	0.17
	0–20	−1.22	3.10	−1.09	2.63	−1.07	2.58	0.33
Porterville	0–7.6	−1.04	2.86	−1.26	2.78	−1.30	2.76	0.18
Reagan	Surface	NC	NC	−1.09	2.83			
Sebree	0–13	−0.47	2.11	−0.53	2.12	−0.51	2.12	0.03
Wasco	0–5.1	−0.93	1.28	−1.19	1.45	−1.38	1.59	0.38
Wyo		−0.58	2.79	−1.05	2.57	−1.13	2.52	0.41
Yolo	0–15	−0.79	3.28	−0.85	3.27	−0.87	3.27	0.04
Midwestern soils								
Bernow	B	0.62	2.85	0.59	2.24	0.56	2.19	0.36
Canisteo	A	NC	NC	−2.51	1.77			
Dennis	A	0.31	2.36	0.38	2.25	0.39	2.23	0.10
	B	NC	NC	1.63	2.19			
Dougherty	A	−1.77	2.11	−1.94	2.14	−2.01	2.14	0.13
Hanlon	A	−0.92	2.50	−0.96	2.37	−0.97	2.34	0.10
Kirkland	A	−0.06	1.76	−0.31	2.21	−0.33	2.24	0.37
Luton	A	−0.79	2.33	−0.59	2.41	−0.55	2.42	0.16
Mansic	A	NC	NC	−0.97	2.21			
	B	NC	NC	−1.78	1.96			
Norge	A	−0.24	2.08	0.06	2.33	0.11	2.35	0.31
Osage	A	0.15	2.13	−0.08	2.57	−0.13	2.63	0.39
	B	0.22	3.24	0.14	2.65	0.13	2.55	0.39
Pond Creek	A	−0.44	2.07	−0.46	2.26	−0.46	2.27	0.11
	B	0.03	1.89	−0.11	2.13	−0.14	2.15	0.21
Pratt	A	−0.99	2.56	−0.92	2.23	−0.89	2.12	0.27
	B	−1.59	2.00	−1.73	2.29	−1.82	2.43	0.33
Richfield	B	−0.77	2.22	−0.40	2.23	−0.37	2.23	0.21
Summit	A	−0.14	2.66	−0.20	2.18	−0.21	2.07	0.33
	B	0.49	1.54	0.44	2.18	0.42	2.34	0.43
Taloka	A	−0.88	2.38	−0.91	2.08	−0.91	2.05	0.18
Teller	A	−1.46	2.15	−1.25	2.11	−1.21	2.11	0.14

[a] NC means that the model could not converge $\log K^2_{Se}$(int) and $\log K_+$(int) simultaneously.

Wichern, 1988). Additionally, a number of the parameter estimates in the $\log K_+$(int) equation appeared to be non-significant. For these reasons the two ANOCOVA models for the two soil groups were optimized separately.

The initial estimate of Eq. (16) for the $\log K^2_{Se}$(int) constant produced an R^2 value of 0.933 and a jack-knifed mean square error (MSE) estimate of 0.089. An initial application of the BWE procedure removed the ln(Al) regression variable for both groups; the secondary application of the PRESS statistic optimization algorithm resulted in the additional removal of the ln(IOC) and ln(CEC) variables and the pooling of the ln(SA) parameter estimate (across groups). The changes in the adjusted R^2 and jack-knifed mean square error (MSE) after each step of the optimization process are shown in Table 3.

Table 3
Regression model identification: summary prediction statistics for each step

Constant	Step	Action	R^2	Adjusted R^2	Jack-knife MSE
$\log K^2_{Se}$	0	Full ANOCOVA model	0.933	0.892	0.089
	1	Removed all ln(Al) parameters	0.932	0.901	0.079
	2	Removed all ln(IOC) parameters	0.915	0.885	0.063
	3	Removed all ln(CEC) parameters	0.915	0.893	0.055
	4	Applied a common ln(SA) parameter constraint	0.912	0.893	0.054
$\log K_+$	0	Full ANOCOVA model	0.633	0.416	0.249
	1	Removed all ln(CEC), ln(OC), and ln(SA) parameters	0.594	0.493	0.172
	2	Constrained Midwestern ln(IOC) parameter to 0	0.594	0.510	0.152
	3	Applied a common ln(Fe) parameter constraint	0.592	0.524	0.129
	4	Constrained Southwestern ln(Al) parameter to 0	0.591	0.538	0.122

After the optimization process was completed, the final estimated prediction equation for the $\log K^2_{Se}(\text{int})$ surface complexation constant was defined to be:

$$\log K^2_{Se}(\text{int}) = \beta_{0j} + \beta_{1j}(\ln \text{OC}) + \beta_{2j}(\ln \text{Fe}) + \beta_3(\ln \text{SA}) + \varepsilon \quad (17)$$

where all but the ln(SA) parameter (β_3) were assumed to be different across groups. This revised model produced an R^2 value of 0.912 and an optimized jack-knifed mean square error (MSE) estimate of 0.054. The corresponding parameter estimates for this model are shown in Table 4. The specific predicted and jack-knife predicted $\log K^2_{Se}(\text{int})$ surface complexation constants for each group of soil samples are shown in Table 2.

The initial estimate of Eq. (16) for $\log K_+(\text{int})$ produced a noticeably lower R^2 value of 0.633 and a larger jack-knifed mean square error (MSE) estimate of 0.249. An application of the BWE procedure on Eq. (16) removed the ln(CEC), ln(SA), and ln(OC) regression variables for both groups, suggesting that the reduced equation should only contain the ln(Al), ln(IOC), and ln(Fe) variables. This reduced, group-specific equation was used as the input model to the PRESS statistic optimization routine. This latter routine identified the ln(IOC) and ln(Al) parameter estimates as dichotomous; setting the Midwestern soil group ln(IOC) and Southwestern soil group ln(Al) estimates to 0, respectively. Additionally, the optimization algorithm pooled the ln(Fe) parameter estimate (across groups). The optimization process stopped after this operation; i.e., no further reduction in the jack-knifed MSE was obtained.

After step 4, the final estimated prediction equation for the $\log K_+(\text{int})$ surface complexation constant was defined to be:

$$\log K_+(\text{int}) = \beta_{0j} + \beta_{1j}(\ln \text{IOC}) + \beta_{2j}(\ln \text{Al}) + \beta_3(\ln \text{Fe}) + \varepsilon \quad (18)$$

with the β_{12} and β_{21} parameters restricted to be 0. This revised model produced an R^2 value of 0.591 and an optimized, jack-knifed mean square error (MSE) estimate of 0.122. The corresponding parameter estimates for this model are shown in Table 4. The specific predicted and jack-knife

Table 4
Regression model summary statistics, parameter estimates, and standard errors

Constant	R^2	Adjusted R^2	MSE	Model F-score	Prob > F
Model summary statistics					
$\log K^2_{Se}$	0.912	0.893	0.045	48.20	<0.0001
$\log K_+$	0.591	0.538	0.103	11.17	<0.0001
Soil group	**Parameter**	**Estimate**	**Standard error**	**t-score**	**Prob > |t|**
$\log K^2_{Se}$ *parameter estimates*					
SW	Intercept	0.675	0.231	2.92	0.007
SW	ln(OC)	−0.083	0.053	−1.56	0.131
SW	ln(Fe)	0.274	0.125	2.20	0.036
MW	Intercept	1.183	0.237	7.65	<0.0001
MW	ln(OC)	−0.470	0.105	−4.45	<0.0001
MW	ln(Fe)	1.033	0.086	12.04	<0.0001
Common	ln(SA)	−0.380	0.051	−7.52	<0.0001
$\log K_+$ *parameter estimates*					
SW	Intercept	3.361	0.164	20.51	<0.0001
SW	ln(IOC)	0.115	0.034	3.42	0.002
MW	Intercept	0.613	0.465	1.32	0.198
MW	ln(Al)	−0.811	0.209	−3.87	0.001
Common	ln(Fe)	0.774	0.169	4.57	<0.0001

predicted $\log K_+$(int) surface complexation constants for each group of soil samples are shown in Table 2.

As shown in Table 4, both regression equations generally exhibit different parameter values across soil groups. Additionally, as shown in Tables 2–4, the $\log K_+$(int) prediction equation appears to be less accurate. This estimated prediction equation exhibits a significantly lower R^2 (0.591 versus 0.912) and larger MSE estimate (0.103 versus 0.045), as compared to the fitted $\log K^2_{Se}$(int) prediction equation. Additionally, an analysis of the soil group specific correlation levels between the numerically optimized and regression model predicted surface complexation constants suggests that the $\log K_+$(int) equation does not predict the Midwestern constants as well ($r = 0.87$ for the Southwestern versus $r = 0.43$ for the Midwestern constants). In contrast, the $\log K^2_{Se}$(int) equation appears to predict the Midwestern constants better ($r = 0.85$ for the Southwestern versus $r = 0.97$ for the Midwestern constants), although both sets of coefficients tend to be accurately predicted for this prediction equation.

A "jack-knifing" procedure was performed on each surface complexation constant regression equation to evaluate its predictive capability. Jack-knifing is a technique where each observation is sequentially set-aside, the regression model is reestimated without the use of this observation, and the set-aside observation is then predicted using the regression model obtained with the remaining data. The final set of 35 jack-knife predicted surface complexation constants is shown in Table 2. The average absolute error (the average of the absolute differences between the optimized versus the jack-knife predicted surface complexation constants) for each soil is also shown. These errors tend to be <0.3 for most of the 35 soils considered in this regression model. The average absolute error across all 35 soils is 0.23 units. Overall, these surface complexation constants appear to be reasonably well estimated. The general good agreement between ordinary predictions and jack-knife estimates suggests that the regression models should have predictive capabilities. The jack-knife MSE estimates for $\log K^2_{Se}$(int) and $\log K_+$(int) were found to be 0.054 and 0.122, respectively. These estimates are sufficiently close to the ordinary MSE estimates of 0.045 and 0.103 produced by the $\log K^2_{Se}$(int) and $\log K_+$(int) equations to also suggest predictive ability and parameter stability.

An analysis of the experimentally measured versus model predicted Se(IV) data was performed to assess both the relative precision and absolute accuracy of the modeling results. The difference between the experimentally determined adsorbed Se(IV) and the adsorbed Se(IV) predicted using the jack-knifed regression model surface complexation constants is defined as:

$$\text{Error\_Ad}_{Se} = \text{Ad}_{Se_m} - \text{Ad}_{Se_e} \tag{19}$$

and the average mean square error, AMSE is:

$$\text{AMSE} = \frac{1}{N}\sum_{i=1}^{N}(\text{Error\_Ad}_{Se})^2 \tag{20}$$

The square root of this latter estimate, ARMSE, was used to quantify square root of the total prediction error. Note that the ARMSE represents the square root of both the prediction variance and the average squared bias effects (Myers and Montgomery, 2002), where the variance and bias reflect the relative precision and absolute accuracy between the experimental and jack-knife predicted Se(IV) adsorption data, respectively. The coefficient-of-imprecision, CIp, a coefficient-of-variation type statistic, was also calculated. It was defined to be:

$$\text{CIp} = \frac{100\text{ARMSE}}{(\overline{Y}_{Se_m} + \overline{Y}_{Se_e})/2} \tag{21}$$

where the denominator represents the average of the two corresponding soil specific mean adsorbed Se(IV) levels. This CIp statistic was used to quantify the relative variation in the adsorbed Se(IV) error distributions with respect to the mean adsorbed Se(IV) levels.

Three types of statistics are shown in Table 5 for each of the 35 calibration soils considered in the study: the ARMSE and CIp estimates (which quantify both relative precision and absolute accuracy) and the Pearson correlation coefficient, CORR (which measures just the relative precision after adjusting out any bias). The adsorption correlation coefficients are all generally quite high; the average correlation

Table 5
Relative precision and absolute accuracy statistics for the experimentally derived versus model predicted Se(IV) adsorption data ($n = 35$ calibration soils)

Soil series	Correlation coefficient	ARMSE (mmol kg^{-1})	CIp
Altamont	0.952	0.0546	49.2
Arlington	0.975	0.0352	33.8
Avon	0.913	0.0215	32.4
Bonsall	0.966	0.0617	52.3
Chino	0.959	0.0256	24.1
Diablo clay	0.825	0.0588	58.1
Diablo clay loam	0.903	0.0631	70.9
Fallbrook	0.969	0.0215	22.7
Fiander	0.983	0.0322	22.9
Pachappa 0–20 cm	0.964	0.0371	27.6
Pachappa 25–51 cm	0.944	0.0601	39.2
Porterville	0.975	0.0654	41.7
Sebree	0.981	0.0239	23.9
Wasco	0.790	0.0577	88.7
Wyo	0.954	0.1266	81.4
Yolo	0.991	0.0290	16.8
Bernow	0.997	0.0229	6.1
Dennis A	0.968	0.0550	19.5
Dougherty	0.876	0.0351	78.0
Hanlon	0.956	0.0294	29.6
Kirkland	0.944	0.0614	33.3
Luton	0.963	0.0656	27.7
Norge	0.982	0.0861	49.7
Osage A	0.975	0.0558	18.6
Osage B	0.968	0.0529	16.8
Pond Creek A	0.931	0.0344	23.3
Pond Creek B	0.983	0.0408	16.2
Pratt A	0.765	0.0139	42.6
Pratt B	0.893	0.0226	46.5
Richfield	0.970	0.0848	42.3
Taloka	0.948	0.0350	23.7
Teller	0.976	0.0513	38.4

level (for all 34 soils) is $r = 0.941$, and 28 of the 34 soils exhibit CORR estimates >0.9. Only one soil exhibits a CORR estimate <0.8 (Pratt A, $r = 0.765$). The ARMSE estimates appear to be quite reasonable, exhibiting an average ARMSE level of 0.0477 mmol kg^{-1}. Only one soil produced an ARMSE estimate >0.1 (Wyo, ARMSE = 0.1266 mmol kg^{-1}). Likewise, the CIp estimates also appear to be very reasonable. That is, the average CIp level is about 37% and 28 of the 35 soils exhibit CIp levels <50%. All of these various summary prediction statistics derived from the jack-knifed constant capacitance model suggest that the corresponding regression equations are both stable and reasonably reliable.

Since the constant capacitance model predictions were generated using the regression model surface complexation constants, one should expect a certain amount of within-soil prediction bias. We tested for this within-soil bias effect by fitting a one-way analysis of variance (ANOVA) model to the error data of Eq. (19). In this ANOVA model, the *F*-test for the soil type effect corresponds to a test for detectable within-soil prediction bias (Montgomery, 1997). The formal test results for this bias are given in the upper portion of Table 6. Note that this ANOVA model explains about 48% of the total error variation, and the *F*-score pertaining to the within-soil bias effect is highly significant ($F = 14.21$, $p < 0.0001$). This apparent bias was also confirmed using a non-parametric Kruskal–Wallis Chi-square test ($\chi^2 = 222.9$, $p < 0.0001$). Not surprisingly, there is a noticeable amount of within-soil prediction bias in the adsorbed Se(IV) errors.

To test for between-soil prediction bias, we calculated the mean adsorption errors for each soil and then analyzed the overall average values of these errors using both a *t*-test and a non-parametric sign-rank test. These test results are shown in the lower portion of Table 6. Both tests suggest that a minimal degree of between-soil prediction bias is present (both tests are significant at the 0.1 level, but not the 0.05 level). A closer examination of these data indicates that the predicted mean adsorption levels tend to be (on average) about 7% lower than the observed mean adsorption levels. In turn, these lower mean levels appear to be caused by an apparent under-estimation bias in the individual lowest adsorption levels (i.e., adsorption levels <0.03 mmol kg^{-1}). In other words, the constant capacitance model predictions generated from the jack-knifed surface complexation constants appear to slightly under-predict the lowest adsorption levels. This low-end prediction bias disappears once the model predictions exceed 0.03 mmol kg^{-1}.

Table 6
Parametric and non-parametric tests for prediction bias in experimentally derived versus constant capacitance model predicted Se(IV) adsorption levels

		Adsorbed Se(IV)
Individual experimental versus model predictions		
ANOVA	*N*	559
	USS/*N*	0.00284 (mmol kg^{-1})
	MSE	0.00152 (mmol kg^{-1})
	R^2	0.480
	F-score	14.21
	ndf, ddf	34, 524
	Probability > *F*	0.0001
Kruskal–Wallis	Chi-square	222.9
	Df	34
	Probability > Chi-square	0.0001
Average error analysis (averaged across soils)		
	N	35
	Mean	0.0110 (mmol kg^{-1})
	Standard error	0.0062 (mmol kg^{-1})
	t-score	1.79
	Probability > |*t*|	0.0819
Signed rank	sr-score	105.0
	Probability > |sr|	0.0854

Figs. 3 and 4 present the ability of the constant capacitance model to predict Se(IV) adsorption from chemical properties for the soils presented in Figs. 1 and 2. For the Midwestern soils, the prediction equations provide descriptions of the experimental adsorption data that are virtually identical in quality to the fits obtained by optimizing the adsorption data (compare Figs. 2 and 4). For the Southwestern soils, the predictions describe the experimental adsorption data less closely than the model fits for most of the soils (compare Figs. 1 and 3). However, the model always correctly predicted the shape of the adsorption envelopes. Since these soils had been used to develop the prediction equations, this evaluation is not an independent assessment of their predictive ability.

The prediction equations were also used to predict surface complexation constants for four soils that had not been used to obtain the general regression model. The constant capacitance model containing these surface complexation constants was used to predict Se(IV) on the four soils. Since the data from the four soils had not been used to develop the prediction equations, this represents an independent evaluation of their ability to predict Se(IV) adsorption. Fig. 5 indicates the ability of this approach to predict

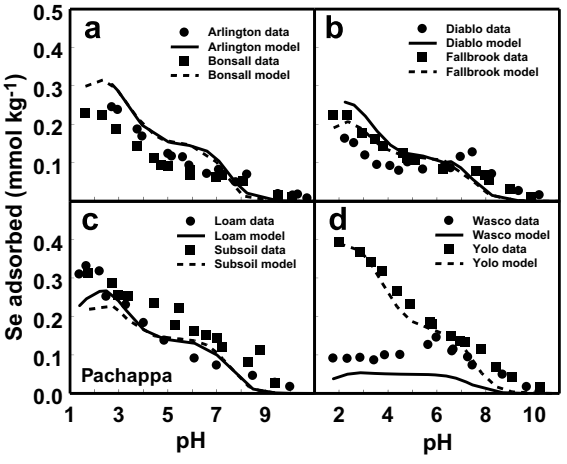

Fig. 3. Prediction of Se(IV) adsorption by Southwestern soils with the constant capacitance model. Experimental data are represented by circles and by squares. Model predictions are represented by solid and dashed lines.

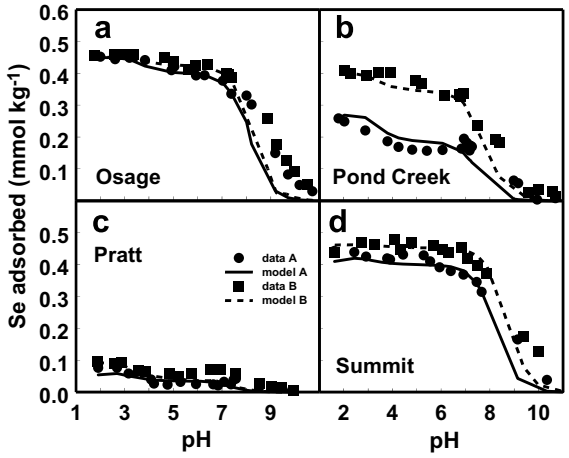

Fig. 4. Prediction of Se(IV) adsorption by Midwestern soils with the constant capacitance model: (a) Osage soil; (b) Pond Creek soil; (c) Pratt soil; and (d) Summit soil. Experimental data are represented by circles for the A horizons and by squares for the B horizons. Model predictions are represented by solid lines for the A horizons and dashed lines for the B horizons.

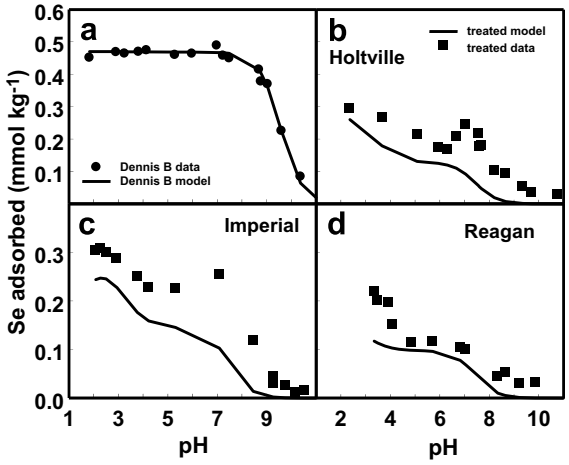

Fig. 5. Prediction of Se(IV) adsorption with the constant capacitance model on soils not used to obtain the prediction equations: (a) Dennis B soil; (b) Holtville soil; (c) Imperial soil; (d) Reagan soil. Experimental data are represented by circles for the untreated samples and by squares for the samples treated to remove carbonates. Model predictions are represented by solid lines.

Se(IV) adsorption on four soils not used to obtain the prediction equations. Prediction of Se(IV) adsorption on the Dennis B soil was excellent (Fig. 5a). The Holtville, Imperial, and Reagan soils all contained >1.6% inorganic carbon and model fitting was not successful. Since application of the surface complexation modeling approach to carbonate systems requires the inclusion of additional surface species: $>CO_3H$, $>CO_3^-$, $>CO_3S^+$, $>SHCO_3$, and $>SCO_3^-$ ($S = Ca$, Mg, etc., van Cappellen et al., 1993), this is not surprising. Selenite adsorption is indicated in Fig. 5b–d for soil samples where carbonates had been removed using a dilute acetate buffer solution. Model predictions of Se(IV) adsorption by the treated soils deviated from the experimental adsorption data by at most about 30%. However, the model was able to accurately predict the shapes of the Se(IV) adsorption envelopes. We consider these results to be reasonable, since they are predictions obtained without optimization of any adjustable parameters. The model predictions were obtained independent of any experimental measurement of Se(IV) adsorption on these soils, using values of easily measured soil chemical parameters. Since our model results are predictions, zero adjustable parameters were used.

4. CONCLUSIONS

The constant capacitance model was able to fit Se(V) adsorption by optimizing one monodentate Se(IV) surface complexation constant and the surface protonation constant. A general regression model was developed for predicting these surface complexation constants from easily measured soil chemical characteristics: inorganic carbon content, organic carbon content, iron oxide content, aluminum oxide content, and surface area. The prediction equations were used to obtain values for the surface complexation constants for four additional soils, providing a completely independent evaluation of the ability of the model to describe Se(IV) adsorption. The present study was carried out at a constant initial Se(IV) concentration. Thus the effect of Se(IV) loading remains to be investigated. Incorporation of these prediction equations into chemical speciation–transport models should allow simulation of Se(IV) behavior on non-calcareous soils under agricultural and environmental conditions. Future research will determine to what extent adequate simulations of Se(IV) adsorption, release, and transport are possible without the need to perform time consuming, detailed adsorption studies for each soil.

ACKNOWLEDGMENTS

Gratitude is expressed to Mr. H.S. Forster, Ms. M.M. Mandap, and Ms. J.M. Mandap for technical assistance, Dr. J.D. Rhoades and Dr. N.T. Basta for providing soil samples, and Mr. S. Nakamura for providing the Nohili soil series classification.

REFERENCES

Adriano D. C. (1986) *Trace Elements in the Terrestrial Environment*. Springer-Verlag, New York.

Anderson P. R. and Benjamin M. M. (1990a) Constant capacitance surface complexation model. Adsorption in silica–iron binary oxide suspensions. *Am. Chem. Soc. Symp. Ser.* **416**, 272–281.

Anderson P. R. and Benjamin M. M. (1990b) Modeling adsorption in aluminum—iron binary oxide suspensions. *Environ. Sci. Technol.* **24**, 1586–1592.

Balistrieri L. S. and Chao T. T. (1990) Adsorption of selenium by amorphous iron oxyhydroxide and manganese dioxide. *Geochim. Cosmochim. Acta* **54**, 739–751.

Balistrieri L. S., Box S. E. and Tonkin J. W. (2003) Modeling precipitation and sorption of elements during mixing of river water and porewater in the Coeur d'Alene River basin. *Environ. Sci. Technol.* **37**, 4694–4701.

Benjamin M. M. (2002) Modeling the mass–action expression for bidentate adsorption. *Environ. Sci. Technol.* **36**, 307–313.

Catalano J. G., Zhang Z., Fenter P. and Bedzyk M. J. (2006) Inner-sphere adsorption geometry of Se(IV) at the hematite (100)–water interface. *J. Colloid Interface Sci.* **297**, 665–671.

Cihacek L. J. and Bremner J. M. (1979) A simplified ethylene glycol monoethyl ether procedure for assessing soil surface area. *Soil Sci. Soc. Am. J.* **43**, 821–822.

Cobo Fernandez M. G., Palacios M. A. and Camara C. (1993) Flow-injection and continuous-flow systems for the determination of Se(IV) and Se(VI) by hydride generation atomic absorption spectrometry with on-line prereduction of Se(VI) to Se(IV). *Anal. Chim. Acta* **283**, 386–392.

Coffin D. E. (1963) A method for the determination of free iron oxide in soils and clays. *Can. J. Soil Sci.* **43**, 7–17.

Davis J. A. and Kent D. B. (1990) Surface complexation modeling in aqueous geochemistry. *Rev. Mineral.* **23**, 177–260.

Del Debbio J. A. (1991) Sorption of strontium, selenium, cadmium, and mercury in soil. *Radiochim. Acta*(52/53), 181–186.

Duc M., Lefevre G., Fedoroff M., Jeanjean J., Ruchard J. C., Monteil-Rivera F., Dumenceau J. and Milonjic S. (2003) Sorption of selenium anionic species on apatites and iron oxides from aqueous solutions. *J. Environ. Radioactivity* **70**, 61–72.

Duc M., Lefevre G. and Fedoroff M. (2006) Sorption of selenite ions on hematite. *J. Colloid Interface Sci.* **298**, 556–563.

Dzombak D. A. and Morel F. M. M. (1990) *Surface Complexation Modeling: Hydrous Ferric Oxide*. John Wiley, New York.

Elsokkary I. H. (1980) Selenium distribution, chemical fractionation and adsorption in some alluvial and lacustrine soils. *Z. Pflanzenernaehr. Bodenk.* **143**, 74–83.

Foster A. L., Brown G. E. and Parks G. A. (2003) X-ray absorption fine structure study of As(V) and Se(IV) sorption complexes on hydrous Mn oxides. *Geochim. Cosmochim. Acta* **67**, 1937–1953.

Fujikawa Y. and Fukui M. (1997) Radionuclide sorption to rocks and minerals: effects of pH and inorganic anions. Part 2. Sorption and speciation of selenium. *Radiochim. Acta* **76**, 163–172.

Ghosh M. M., Cox C. D. and Yuan-Pan J. R. (1994) Adsorption of selenium on hydrous alumina. *Environ. Progress* **13**, 79–88.

Girling C. A. (1984) Selenium in agriculture and the environment. *Agric. Ecosyst. Environ.* **11**, 37–65.

Goldberg S. (1991) Sensitivity of surface complexation modeling to the surface site density parameter. *J. Colloid Interface Sci.* **145**, 1–9.

Goldberg S. (1992) Use of surface complexation models in soil chemical systems. *Adv. Agron.* **47**, 233–329.

Goldberg S. and Glaubig R. A. (1988) Anion sorption on a calcareous, montmorillonitic soil—selenium. *Soil Sci. Soc. Am. J.* **52**, 954–958.

Goldberg S. and Sposito G. (1984) A chemical model of phosphate adsorption by soils. I. Reference oxide minerals. *Soil Sci. Soc. Am. J.* **48**, 772–778.

Goldberg S., Lesch S. M. and Suarez D. L. (2000) Predicting boron adsorption by soils using soil chemical parameters in the constant capacitance model. *Soil Sci. Soc. Am. J.* **64**, 1356–1363.

Goldberg S., Lesch S. M. and Suarez D. L. (2002) Predicting molybdenum adsorption by soils using soil chemical parameters in the constant capacitance model. *Soil Sci. Soc. Am. J.* **66**, 1836–1842.

Goldberg S., Suarez D. L., Basta N. T. and Lesch S. M. (2004) Predicting boron adsorption isotherms by Midwestern soils using the constant capacitance model. *Soil Sci. Soc. Am. J.* **68**, 795–801.

Goldberg S., Lesch S. M., Suarez D. L. and Basta N. T. (2005) Predicting arsenate adsorption by soils using soil chemical parameters in the constant capacitance model. *Soil Sci. Soc. Am. J.* **69**, 1389–1398.

Goldberg S., Martens D. A., Forster H. S. and Herbel M. J. (2006) Speciation of selenium(IV) and selenium(VI) using coupled ion chromatography—hydride generation atomic absorption spectrometry. *Soil Sci. Soc. Am. J.* **70**, 41–47.

Harr J. R. (1978) Biological effects of selenium. In *Toxicity of Heavy Metals in the Environment Part 1* (ed. F. W. Oehme). Marcel Dekker, New York, pp. 393–426.

Hayes K. F., Roe A. L., Brown G. E., Hodgson K. O., Leckie J. O. and Parks G. A. (1987) In situ X-ray absorption study of surface complexes: Selenium oxyanions on α-FeOOH. *Science* **238**, 783–786.

Hayes K. F., Papelis C. and Leckie J. O. (1988) Modeling ionic strength effects on anion adsorption at hydrous oxide/solution interfaces. *J. Colloid Interface Sci.* **125**, 717–726.

Herbelin A. L. and Westall J. C. (1996) FITEQL: a computer program for determination of chemical equilibrium constants from experimental data. Rep. 96-01, Version 3.2, Department of Chemistry, Oregon State University, Corvallis.

Hiemstra T. and van Riemsdijk W. H. (1999) Surface structural ion adsorption modeling of competitive binding of oxyanions by metal (hydr)oxides. *J. Colloid Interface Sci.* **210**, 182–193.

Johnson R. A. and Wichern D. W. (1988) *Applied Multivariate Statistical Analysis*, second ed. Prentice Hall, Englewood Cliffs.

Lakin H. W. (1961) Selenium Content of Soils. USDA-ARS Agric. Handb. 200. U.S. Gov. Print. Office, Washington.

Levesque M. (1974) Selenium distribution in Canadian soil profiles. *Can. J. Soil Sci.* **54**, 63–68.

Kunze G. W. and Dixon J. B. (1986) Pretreatment for mineralogical analysis. In *Methods of Soil Analysis*, Part 2, second ed. (eds. A. L. Page et al.) Agron. Monogr. 9. American Society of Agronomy, Madison, pp. 91–100.

Manceau A. and Charlet L. (1994) The mechanism of selenate adsorption on goethite and hydrous ferric oxide. *J. Colloid Interface Sci.* **168**, 87–93.

Martinez M., Gimenez J., de Pablo J., Rovira M. and Duro L. (2006) Sorption of selenium(IV) and selenium(VI) onto magnetite. *Appl. Surf. Sci.* **252**, 3767–3773.

Masscheleyn P. H., Delaune R. D. and Patrick W. H. (1990) Transformations of selenium as affected by sediment oxidation–reduction potential and pH. *Environ. Sci. Technol.* **24**, 91–96.

Montgomery D. C. (1997) *Design and Analysis of Experiments*, fifth ed. John Wiley, New York.

Myers R. H. (1986) *Classical and Modern Regression with Applications*. Duxbury Press, Boston.

Myers R. H. and Montgomery D. C. (2002) *Response Surface Methodology: Process and Product Optimization Using Designed Experiments*. John Wiley, New York.

Neal R. H. and Sposito G. (1989) Selenate adsorption on alluvial soils. *Soil Sci. Soc. Am. J.* **53**, 70–74.

Ohlendorf H. M., Hoffman D. J., Saiki M. K. and Aldrich T. W. (1986) Embryonic mortality and abnormalities of aquatic birds: apparent impacts of selenium from irrigation drainwater. *Sci. Total Environ.* **52**, 49–63.

Papelis C., Brown G. E., Parks G. A. and Leckie J. O. (1995) X-ray absorption spectroscopic studies of cadmium and selenite adsorption on aluminum oxides. *Langmuir* **11**, 2041–2048.

Peak D. (2006) Adsorption mechanisms of selenium oxyanions at the aluminum oxide/water interface. *J. Colloid Interface Sci.* **303**, 337–345.

Peak D., Saha U. K. and Huang P. M. (2006) Selenite adsorption mechanisms on pure and coated montmorillonite: an EXAFS and XANES study. *Soil Sci. Soc. Am. J.* **70**, 192–203.

Rhoades J. D. (1982) Cation exchange capacity. In *Methods of Soil Analysis*. Part 2, second ed. (eds. A. L. Page et al.). Agron. Monogr. 9. American Society of Agronomy, Madison, pp. 149–157.

Saeki K. and Matsumoto S. (1994) Influence of organic matter on selenite sorption by andosols. *Commun. Soil Sci. Plant Anal.* **25**, 3379–3391.

SAS (1999) SAS/STAT Users Guide, Version 8. SAS Institute Inc., Cary.

Singh M., Singh N. and Relan P. S. (1981) Adsorption and desorption of selenite and selenate selenium on different soils. *Soil Sci.* **132**, 134–141.

Sposito G. (1983) Foundations of surface complexation models of the oxide–aqueous solution interface. *J. Colloid Interface Sci.* **91**, 329–340.

Sposito G., de Wit J. C. M. and Neal R. H. (1988) Selenite adsorption on alluvial soils: III. Chemical modeling. *Soil Sci. Soc. Am. J.* **52**, 947–950.

Thomas G. W. (1996) Soil pH and soil acidity. In Methods of Soil Analysis Part 3—Chemical Methods. In *Soil Science Society of America Book Series 5* (ed. D. L. Sparks et al.). Soil Science Society of America, Madison, pp. 475–490.

van Cappellen P., Charlet L., Stumm W. and Wersin P. (1993) A surface complexation model of the carbonate mineral–aqueous solution interface. *Geochim. Cosmochim. Acta* **57**, 3505–3518.

Wang X. and Liu X. (2005) Sorption and desorption of radioselenium on calcareous soil and its solid components studied by batch and column experiments. *Appl. Radiot. Isot.* **62**, 1–9.

Westall J. and Hohl H. (1980) A comparison of electrostatic models for the oxide/solution interface. *Adv. Colloid Interface Sci.* **12**, 265–294.

Zhang P. and Sparks D. L. (1990) Kinetics of selenate and selenite adsorption/desorption at the goethite/water interface. *Environ. Sci. Technol.* **24**, 1848–1856.

Associate editor: Stephan M. Kraemer